Inorganic Chemistry

Article

pubs.acs.org/IC

Electrocatalytic Hydrogen Evolution from Water by a Series of Iron Carbonyl Clusters

An D. Nguyen,[†] M. Diego Rail,[†] Maheswaran Shanmugam, James C. Fettinger, and Louise A. Berben*

Department of Chemistry, University of California, Davis, California 95616, United States

Supporting Information

ABSTRACT: The development of efficient hydrogen evolving electrocatalysts that operate near neutral pH in aqueous solution remains of significant interest. A series of low-valent iron clusters have been investigated to provide insight into the structure−function relationships affecting their ability to promote formation of cluster-hydride intermediates and to promote electrocatalytic hydrogen evolution from water. Each of the metal carbonyl anions, $[Fe_4N(CO)_{12}]^-$ ($\mathbf{1}^-$), $[Fe_4C(CO)_{12}]^{2-}$ ($\mathbf{2}^{2-}$), $[Fe_5C(CO)_{15}]^{2-}$ ($\mathbf{3}^{2-}$), and $[Fe_6C(CO)_{18}]^{2-}$ ($\mathbf{4}^{2-}$) were isolated as their sodium salt to provide the necessary solubility in water. At pH 5 and −1.25 V vs SCE the clusters afford hydrogen with Faradaic efficiencies ranging from 53−98%. pH dependent cyclic voltammetry measurements provide insight into catalytic intermediates. Both of the butterfly shaped clusters, $\mathbf{1}^-$ and $\mathbf{2}^{2-}$, stabilize protonated adducts and are effective catalysts. Initial reduction of butterfly shaped $\mathbf{1}^-$ is pH-independent and subsequently, successive protonation events afford $H\mathbf{1}^-$, and then hydrogen. In contrast, butterfly shaped $\mathbf{2}^{2-}$ undergoes two successive proton coupled electron transfer events to form $H_2\mathbf{2}^{2-}$ which then liberates hydrogen. The higher nuclearity clusters, $\mathbf{3}^{2-}$ and $\mathbf{4}^{2-}$, do not display the same ability to associate with protons, and accordingly, they produce hydrogen less efficiently.

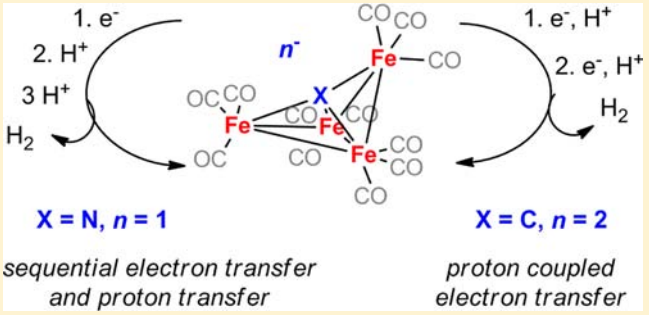

INTRODUCTION

Hydrogen has the potential to provide a transportable, high density form of energy storage for use as a fuel or as a reagent in commodity chemical synthesis. Electrocatalysis is an appealing means for producing hydrogen because it will facilitate conversion of electrons derived from renewable sources, such as solar or wind, into easily storable energy. The use of aqueous media is important if proton reduction will ultimately be coupled with water oxidation in a closed cycle device. Cobalt and nickel complexes feature prominently as examples of earth abundant, molecular hydrogen evolving electrocatalysts that operate in aqueous media, and progress continues to be made in this area.[1] However, the lower cost and far higher natural abundance of iron make the study of iron-based molecular electro-reduction catalysts potentially even more appealing.

There are notably few reports of iron electrocatalysts that are compatible with aqueous solution. A handful of iron-based electrocatalysts have been studied in nonaqueous solution, and this includes original work by Saveant et al.,[2] and more recent studies reported by Ott et al.,[3] and by Rose and Gray.[4] In addition, an extensive collection of work inspired by biomimetic interest in binuclear, low-valent iron complexes, that have been synthesized to model the structure and function of the diiron hydrogenase enzyme, exists. Many important contributions have been made in this field,[5,6] and in some instances the model systems are compatible with water-organic mixtures.[7] Examples of iron electrocatalysts compatible with aqueous-only solution include a report by Pickett that dianionic $(\mu\text{-pdt})[Fe(CO)_2CN]_2^{2-}$ was highly water-soluble (μ-pdt = $-S(CH_2)_3S-$) although it did not electrocatalytically reduce protons between pH 4−8.4.[8] Darensbourg has studied arylsulfonyl-appended Fe_2 electrocatalysts that were water-soluble and interacted with cyclodextrins, and showed some activity toward acetic acid in aqueous solution at −1.45 V vs SCE.[9] In a similar vein, Gloaguen reported that sodium dodecyl sulfate surfactant (SDS) could be used to dissolve $Fe_2(bdt)(CO)_6$ (bdt = benzenedithiolate) in water, and that this catalyst reduced the protons in HOAc in unbuffered aqueous solutions, particularly at pH 3.[10]

An efficient and stable water-soluble iron electrocatalyst that operates at modest potentials is still a desirable goal. Herein, we report on a series of low-valent multinuclear iron clusters for electrocatalytic proton reduction in aqueous media. Structure−function relationships can shed light on mechanistic details and important electrocatalyst design criteria and so we have studied a nitride-containing four iron cluster, along with carbide containing clusters of four, five, and six iron centers: $[Fe_4N(CO)_{12}]^-$ ($\mathbf{1}^-$), $[Fe_4C(CO)_{12}]^{2-}$ ($\mathbf{2}^{2-}$), $[Fe_5C(CO)_{15}]^{2-}$ ($\mathbf{3}^{2-}$), and $[Fe_6C(CO)_{18}]^{2-}$ ($\mathbf{4}^{2-}$) (Chart 1). We discuss the electron transfer and proton-coupled electron transfer (PCET)

Received: September 20, 2013
Published: October 11, 2013

   dx.doi.org/10.1021/ic4023882 | Inorg. Chem. 2013, 52, 12847−12854

Chart 1

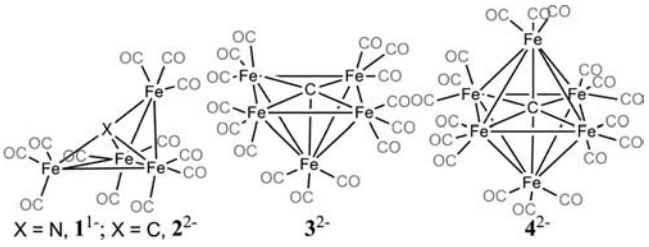

events that are accessible via cyclic voltammetry (CV) between pH 5−9. Based on these observations, we have correlated the charge of the clusters with their relative ability to stabilize protonated intermediates which in turn correlates with their ability to catalyze hydrogen evolution. The butterfly shaped clusters $\mathbf{1}^-$ and $\mathbf{2}^{2-}$ catalyze hydrogen evolution from aqueous solutions at −1.25 V vs SCE with 98 and 85% Faradaic efficiency, respectively. Clusters $\mathbf{3}^{2-}$ and $\mathbf{4}^{2-}$ did not form hydride intermediates, and were correspondingly less effective for hydrogen evolution and operated at 72% and 64% Faradaic efficiency, respectively.

RESULTS AND DISCUSSION

Synthesis and Characterization of Clusters. The sodium salt of nitride containing $\mathbf{1}^-$ was obtained from an aqueous solution workup of $\mathbf{1}^-$ following its synthesis via a modified literature procedure.[11] A single crystal X-ray diffraction analysis of the compound was undertaken on crystals grown by diffusion of tetrahydrofuran (THF) into an aqueous solution to probe possible interactions between the sodium ion and the cluster $\mathbf{1}^-$ (Supporting Information, Table S1). The solid state structure of $\mathbf{1}^-$ revealed that two diglyme molecules, which originate from the synthesis of $\mathbf{1}^-$ encapsulate the sodium ion so that $[diglyme_2Na]^+$ is well separated from the anionic cluster and should not influence the reactivity of $[diglyme_2Na]$-**1** in solution (Figure 1). All bond lengths and angles in the cluster core are in accord with previously reported salts of $\mathbf{1}^-$ (Supporting Information, Figure S1).

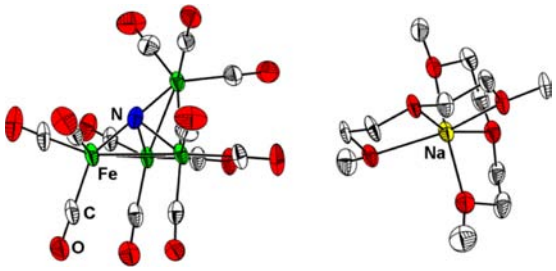

Figure 1. Structure of $[diglyme_2Na][Fe_4N(CO)_{12}]$ ($[diglyme_2$-Na]-**1**). Green, white, red, blue, and yellow colors indicate Fe, C, O, N, and Na atoms, respectively. Thermal ellipsoids at 40% probability; H atoms omitted.

The carbide containing Et_4N^+ and Na^+ salts of $\mathbf{2}^{2-}$,[12] $\mathbf{3}^{2-}$,[13] and $\mathbf{4}^{2-}$,[14] were each prepared by procedures modified from literature reports for the PPN salts of the clusters (PPN = bis(triphenylphosphine)iminium, Chart 1). In the syntheses we performed, a formulation for the sodium countercations which incorporates two molecules of diglyme: $[diglyme_2Na]_2$-**2**, or 3 molecules of DME: $[DME_3Na]_2$-**3**, and $[DME_3Na]_2$-**4**, per sodium cation is consistent with elemental analysis data and with the integration against internal standards we observed via ^{1}H NMR spectroscopy (Supporting Information, Figure S2). The structures of clusters $\mathbf{1}^-$ and $\mathbf{2}^{2-}$ are best described as butterfly shaped, $\mathbf{3}^{2-}$ is square pyramidal, and $\mathbf{4}^{2-}$ is octahedral.

Electrochemical Characterization of Clusters. CV experiments on $\mathbf{1}^-$−$\mathbf{4}^{2-}$ were performed at pH 2, 5, 7, and 9. CV scans at pH 2 showed anomalous behavior as compared to other pH values, and we attributed this to decomposition of the clusters at low pH. Background CV scans of the buffers with no cluster added indicated that no redox events occurred in the absence of cluster (Supporting Information, Figure S3). Based on the CVs of $\mathbf{1}^-$−$\mathbf{4}^{2-}$ (Figures 2−4, and 6), plots of peak

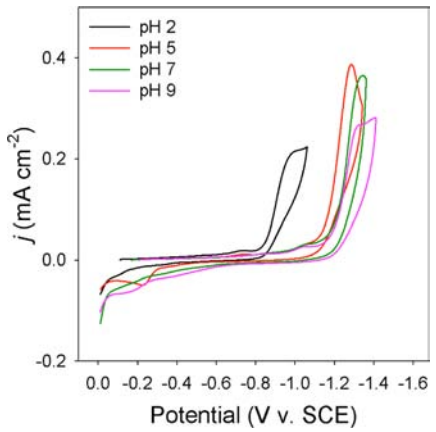

Figure 2. CVs of 0.15 mM $\mathbf{1}^-$ in various buffered solutions from pH 2−9. 100 mV/s, GC electrode. Scans initiated at the open circuit potential for each pH value.

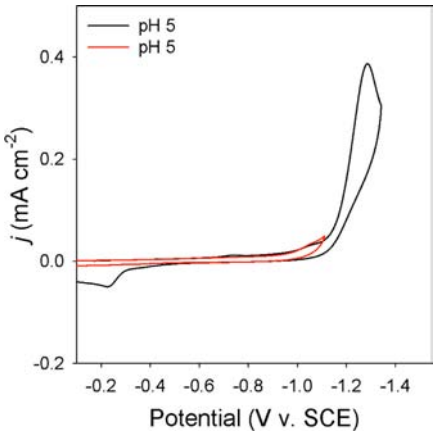

Figure 3. CV of 0.15 mM $\mathbf{1}^-$ at pH 5 with scan reversed at −1.1 V (red), −1.4 V (black). 100 mV/s, GC electrode.

current vs square root of the scan rate were compiled for the most distinctive feature in the cathodic region for each of the clusters at pH 7, and their linear nature indicated that the observed redox events are associated with clusters dissolved in a homogeneous solution (Supporting Information, Figures S4, S5).[15] In all cases the reduction events associated with $\mathbf{1}^-$−$\mathbf{4}^{2-}$ are irreversible which is consistent with electrocatalytic hydrogen evolution (vide infra).

The CV of $\mathbf{1}^-$ displayed an irreversible reduction event at −1.25 V vs SCE which retained a relatively constant current density response and reduction potential over the pH range of 5 to 9 (Figure 2, see Experimental Section for details of the

dx.doi.org/10.1021/ic4023882 | Inorg. Chem. 2013, 52, 12847−12854

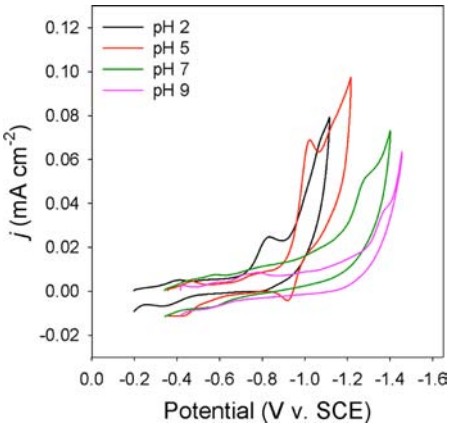

Figure 4. CVs of 0.15 mM 2^{2-} in various buffered solutions from pH 2–9. 100 mV/s, GC electrode. Scans initiated at the open circuit potential for each pH value. Initial redox events at −0.36 (pH 2), −0.47 (pH 5), −0.60 (pH 7), and −0.73 V (pH 9); catalytic events at −0.85 V (pH 2), −1.07 V (pH 5), −1.23 V (pH 7), and −1.37 V (pH 9).

buffers). The observation of one consistent reduction event over the pH range of 5–9 implies that the reduction of $\mathbf{1}^-$ is not proton coupled over this range and that the redox event at −1.25 V corresponds to the process

$$[Fe_4N(CO)_{12}]^- + e \rightarrow [Fe_4N(CO)_{12}]^{2-} \quad (1)$$

The large shift in the reductive peak position at pH 2, combined with a change in the solution color, implied that $\mathbf{1}^-$ is not stable to solutions of pH 2. On the reverse, anodic scan an irreversible oxidation event at −0.25 V was observed at pH 5. Reduction and oxidation cycles were performed at pH 5 where the change in the scan direction occurred at different potentials. This experiment showed that the oxidation event at −0.25 V is only apparent if the reducing scan extends beyond the reduction event at −1.25 V (Figure 3). We propose that following reduction of $\mathbf{1}^-$ to $\mathbf{1}^{2-}$ the cluster is protonated to afford $H\mathbf{1}^-$, and that the oxidation event at −0.25 V corresponds to oxidation of $H\mathbf{1}^-$ according to the reactions

$$[Fe_4N(CO)_{12}]^{2-} + H^+ \rightarrow [HFe_4N(CO)_{12}]^- \quad (2)$$

$$[HFe_4N(CO)_{12}]^- \rightarrow [HFe_4N(CO)_{12}] + e \quad (3)$$

We have observed a similar sequence of events when $\mathbf{1}^-$ was studied in MeCN solution in the presence of organic acids and in that case we confirmed the identity of the oxidation event by synthesis of an authentic sample of $H\mathbf{1}$.[16] In the present experiments, the observation of $H\mathbf{1}^-$ is pH dependent. Above pH 7, the event at −0.25 V is not observed: this result is consistent with very slow formation of $H\mathbf{1}^-$ under the conditions of low proton availability so that $H\mathbf{1}^-$ does not build up in solution in sufficient quantities to be observed on the return scan near −0.25 V. At pH 5 we propose that the rate of formation of $H\mathbf{1}^-$ is faster than the subsequent reaction of $H\mathbf{1}^-$ with another proton and so observation of $H\mathbf{1}^-$ electrochemically is possible.

Whereas $\mathbf{1}^-$ was consistently reduced by one-electron at potentials close to −1.22 V over all pH values, the carbide-containing clusters $\mathbf{2}^{2-}$–$\mathbf{4}^{2-}$ displayed more variable reduction events (Figures 4–6). In some cases variability in CVs with pH suggested the presence of protonated cluster adducts in solution, and the observed difference in the proton dependence of the reduction events for $\mathbf{1}^-$ vs $\mathbf{2}^{2-}$ is consistent with the difference in charge on the clusters. Nitride-centered $\mathbf{1}^-$ is protonated after reduction to $\mathbf{1}^{2-}$, whereas carbide-centered $\mathbf{2}^{2-}$ is protonated concurrent with reduction.

Butterfly shaped $\mathbf{2}^{2-}$ displayed no reduction event that could be reasonably assigned to reduction of the unprotonated cluster, $\mathbf{2}^{2-}$. Low current density reduction events for $\mathbf{2}^{2-}$ were observed at fairly positive potentials: at −0.36 (pH 2), −0.47 (pH 5), −0.60 (pH 7), and −0.73 V (pH 9).[17] The −55 mV per pH unit dependence of this reversible redox event is close to the Nernstian response of −60 mV per pH unit expected for a one-electron and one-proton reduction (Figure 5, left).[18] Moreover, the low current density and reversibility of the waves suggest that no electrocatalytic event occurs at these redox events and we assign these processes to a reversible two electron reduction of $\mathbf{2}^{2-}$ that is coupled with a protonation event

$$[Fe_4C(CO)_{12}]^{2-} + H^+ + e \rightarrow [HFe_4C(CO)_{12}]^{2-} \quad (4)$$

A second series of distinct proton-dependent reduction features between pH 2–9 (Figure 4) were also observed. We ascribe the electrochemical features at −0.85 V (pH 2), −1.07 V (pH 5), −1.23 V (pH 7), and −1.37 V (pH 9) to a proton coupled one-electron reduction event which is consistent with the 74 mV per pH unit shift to higher potential observed with

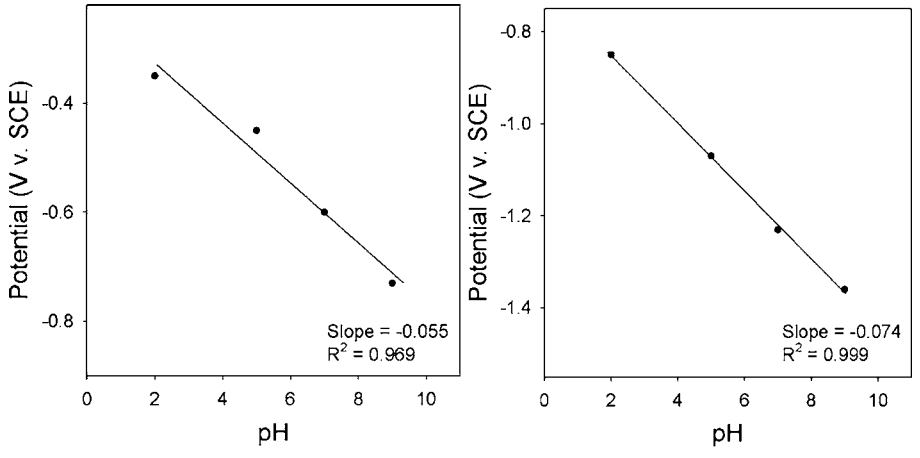

Figure 5. Plots of potential vs pH (left) for the reversible redox process for $\mathbf{2}^{2-}$, and (right) for the irreversible, catalytic process for $\mathbf{2}^{2-}$.

dx.doi.org/10.1021/ic4023882 | Inorg. Chem. 2013, 52, 12847–12854

lower proton availability which should theoretically occur at a rate of 60 mV per pH unit (Figure 5, right). This reaction corresponds to formation of $[H_2Fe_4C(CO)_{12}]^{3-}$, which then presumably loses H_2 electrocatalytically. The assignment of these redox events to a catalytic event is supported by the large increase in current density:

$$[HFe_4C(CO)_{12}]^{2-} + H^+ + e \rightarrow [H_2Fe_4C(CO)_{12}]^{2-} \quad (5)$$

$$[H_2Fe_4C(CO)_{12}]^{2-} \rightarrow [Fe_4C(CO)_{12}]^{2-} + H_2 \quad (6)$$

Protonation of 2^{2-} in organic solution has precedent.[19] Formation of $[HFe_4C(CO)_{12}]^-$ from $[Fe_4C(CO)_{12}]^{2-}$ occurs in organic solution in the presence of strong acids such as CF_3SO_3H and the proton resides μ^2-Fe_2 along the butterfly "hinge" (Chart 2). Further protonation, upon reaction of

Chart 2

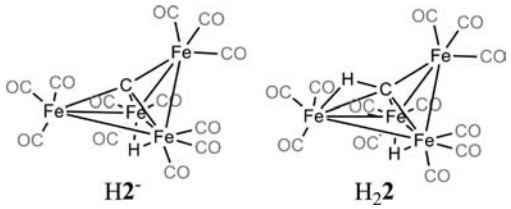

$[HFe_4C(CO)_{12}]^-$ with a second equivalent of CF_3SO_3H, affords $[HFe_4(\mu^2\text{-}CH)(CO)_{12}]$ where the second proton bridges the carbide and an iron center (Chart 2). In the present work, the pH dependence of the redox events indicated that reduction of 2^{2-} was coupled with protonation events. Thus, protonation of 2^{2-} can occur under fairly mild conditions near neutral pH upon reduction of the cluster. We speculate that the first proton bridges the Fe–Fe bond on the butterfly hinge, and that the second proton is most likely to interact with the first proton so that their interaction leads to hydrogen formation. Similarly rich protonation and hydride formation chemistry has been documented in model complexes of the diiron hydrogenase enzymes.[5,20]

There is a noticeable variation in the current density with respect to pH observed for the proton coupled redox processes described for 2^{2-}. Current density is a function of the rate of the catalytic reaction and so it is apparent from the CVs that the fastest rate of hydrogen evolution is observed at pH 5 (vide infra). At higher pH values, 7 and 9, the current density decreases with increasing pH, and this indicates that the rate of the catalytic reaction decreases as the proton availability in solution decreases. The current density at pH 2 does not follow this trend in catalytic rates, and we attribute this to decomposition of 2^{2-} under acidic conditions. Indeed, solutions of 2^{2-} at pH 2 lose their peach color over the course of 5 h: between pH 5–9 the peach color remains intact for longer than 24 h.

The CV scans of square pyramidal 3^{2-} and octahedral 4^{2-} between pH 5–9 (Figure 6) include an irreversible reduction process at −1.32, and −1.36 V, respectively, that is pH independent, and could reasonably correspond to the reactions

$$[Fe_5C(CO)_{15}]^{2-} + e \rightarrow [Fe_5C(CO)_{15}]^{3-} \quad (7)$$

$$[Fe_6C(CO)_{18}]^{2-} + e \rightarrow [Fe_6C(CO)_{18}]^{3-} \quad (8)$$

The observation of a pH-independent event within the solvent window is consistent with the greater ability of

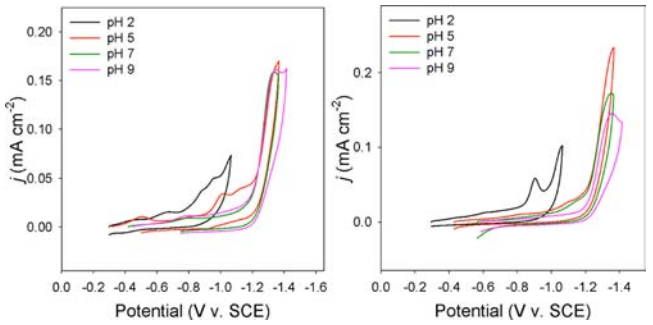

Figure 6. CVs of 3^{2-} (left) and 4^{2-} (right) in various buffered solutions from pH 2–9. 100 mV/s, GC electrode. Scans were initiated at the open circuit potential for each pH value.

pentanuclear 3^{2-} and hexanuclear 4^{2-} to delocalize charge, as compared with tetranuclear 2^{2-}: a higher degree of delocalization of charge is credited with the easily accessible reduction processes. Additional reduction events for 3^{2-} were observed at −0.90 V (pH 2), and at −1.03 V (pH 5), and 4^{2-} displayed a further reduction event at −0.90 V (pH 2). We ascribe these events to reduction of 2^{2-} which has formed by rearrangement of 3^{2-} and 4^{2-} under the influence of protons. The CVs for 2^{2-} described earlier showed evidence for protonation of 2^{2-} under conditions of pH 7 or lower and so it is reasonable that 3^{2-} and 4^{2-} also associate with protons under similar pH conditions. It is known that 3^{2-} and 4^{2-} rearrange to 2^{2-} in the presence of acid,[21] and indeed, over longer time periods we observed that violet solutions of 3^{2-} and deep burgundy solutions of 4^{2-} become the peach color of 2^{2-}.

Hydrogen Evolution. The production of hydrogen by each cluster was interrogated using controlled potential electrolysis (CPE) experiments. The most informative CPE measurements were those carried out at pH 5, 7 and 9, at −1.25 V vs SCE, in 0.1 M $NaClO_4$ solution with added 4 mM of the appropriate buffer in a sealed electrochemical cell (Table 1 and Supporting

Table 1. Results from CPE Experiments with 0.15 mM Catalyst in 0.1 M $NaClO_4$/4 mM pH 5 Acetate Buffer over 2.5 h[a]

catalyst	q (C)[b]	Faradaic yield	TON[c]
none	1.0		
1^-	68	98	34
2^{2-}	38	83	16
3^{2-}	13	72	5
4^{2-}	10	64	8

[a]Glassy carbon working electrode surface area = 23 cm^2. Results are averages from at least 2 trials for each catalyst. [b]Charge passed during CPE experiment. [c]Turnover number (TON) is moles of H_2 per mole of catalyst over 2.5 h.

Information, Table S2). During these experiments the headspace was sampled using a gastight syringe and analyzed by GC-TCD. Experiments performed at −1.25 V correspond to an overpotential (η) of 714 mV for pH 5, 594 mV for pH 7, and 474 mV for pH 9.[22] Moreover, at −1.25 V vs SCE, catalysis is compatible with use of a glassy carbon electrode in the pH range 5–9. Control experiments under these pH conditions demonstrated that very little charge is passed in the absence of catalyst (Table 1 and Supporting Information, Table S2, Figure 7). CPE experiments performed with $Na_2[Fe(CO)_4]$ and $Fe(NO_3)_3$ afforded H_2 with only 35 and 20% Faradaic

dx.doi.org/10.1021/ic4023882 | Inorg. Chem. 2013, 52, 12847–12854

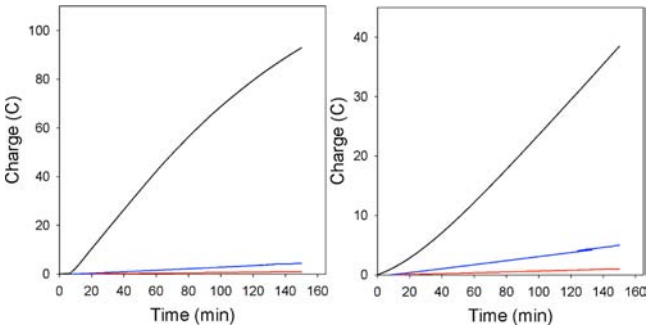

Figure 7. Charge vs time plots for CPE experiments with $\mathbf{1}^{-}$ (left) and $\mathbf{2}^{2-}$ (right) (black lines); with no catalyst (red lines); and with a rinsed electrode from an experiment with $\mathbf{1}^{-}$ and $\mathbf{2}^{2-}$ run in fresh electrolyte solution to demonstrate that no catalyst plated on the electrode (blue lines).

efficiency, respectively, and very little charge was passed (Supporting Information, Table S2). Reported catalysts that operate at more negative potentials require the use of mercury working electrodes to avoid background hydrogen evolution at the glassy carbon electrode.

Both of the butterfly shaped clusters $\mathbf{1}^{-}$ and $\mathbf{2}^{2-}$ were the most effective for hydrogen evolution out of the clusters that we studied. Nitride-containing $\mathbf{1}^{-}$ catalyzed liberation of hydrogen with 98 ± 3% Faradaic efficiency over the pH range 5−9 and operated with a current density of roughly 0.1 mA/cm^2. The rate of hydrogen evolution was pH dependent (i.e., overpotential dependent) and the fastest catalysis was observed at pH 5 where 68 C of charge were passed over 2.5 h (Figure 7, left). At pH 9 just 10 C of charge were passed over the same time period. Carbide containing $\mathbf{2}^{2-}$ liberated hydrogen with 85 ± 3% Faradaic efficiency at pH 5 and 7, and this efficiency dropped to 55 ± 3% at pH 9. The rate of catalysis by $\mathbf{2}^{2-}$ was somewhat slower than we observed for $\mathbf{1}^{-}$ which operated at roughly 0.06 mA/cm^2 under conditions of our experiment and 38 C of charge were passed over 2.5 h at pH 5 (Figure 7, right). CPE experiments on $\mathbf{1}^{-}$ and $\mathbf{2}^{2-}$ at pH 5 and −1.25 V were run over 24 h to ascertain that the catalysts were stable in solution: the rate of reaction remained fairly constant over the 24 h period, as did the color of the solution.

Following CPE measurements using $\mathbf{1}^{-}$ (or $\mathbf{2}^{2-}$), the same glassy carbon electrode was introduced into a buffered solution absent of $\mathbf{1}^{-}$ (or $\mathbf{2}^{2-}$) and retested for hydrogen evolution reaction (HER) at −1.25 V to probe the possibility that $\mathbf{1}^{-}$ (or $\mathbf{2}^{2-}$) may reductively plate onto the GC electrode during CPE experiments. The electrode was found to be similar in its effectiveness for catalysis as a freshly polished GC electrode (Figure 7). This observation confirms that the active catalyst in each case is the cluster in solution rather than a surface absorbed species. We also performed an experiment where additional $\mathbf{1}^{-}$ (or $\mathbf{2}^{2-}$) was injected into a CPE experiment after 30 min of operation. Upon injection of the aliquot, the current density immediately increased and indicated that catalyst in solution was responsible for HER. Potential catalysis by iron nanoparticles formed from $\mathbf{1}^{-}$ was probed by a CPE experiment in the presence of elemental mercury: no change compared to experiments without mercury was observed. A subsequent CPE with the same mercury and no $\mathbf{1}^{-}$ evolved no more H_2 than a typical blank experiment.

CPE experiments with $\mathbf{3}^{2-}$ and $\mathbf{4}^{2-}$ indicated that these clusters are less efficient electrocatalysts for hydrogen evolution than either $\mathbf{1}^{-}$ or $\mathbf{2}^{2-}$. Hydrogen evolution by $\mathbf{3}^{2-}$ and $\mathbf{4}^{2-}$ at pH 5 and −1.25 V occurred with Faradaic efficiencies of 72 ± 5% and 63 ± 5%, respectively. The rates for each of the reactions were slower as well; 13 and 10 C of charge were passed over 2.5 h by $\mathbf{3}^{2-}$ and $\mathbf{4}^{2-}$, respectively. It should also be noted that, since $\mathbf{3}^{2-}$ and $\mathbf{4}^{2-}$ are known to slowly rearrange to $\mathbf{2}^{2-}$ some of the hydrogen detected in these experiments may have been formed in a reaction catalyzed by $\mathbf{2}^{2-}$.

The integrity of the most efficient clusters $\mathbf{1}^{-}$ and $\mathbf{2}^{2-}$ was investigated following CPE measurements using IR spectroscopy. Measurements were performed on a solution aliquot of the reaction mixture before and after the CPE experiment. The carbonyl region of the spectra obtained before and after CPE show no difference in either the frequency or intensity of the absorption bands and this, in conjunction with consistent color of the CPE solution, indicated that $\mathbf{1}^{-}$ and $\mathbf{2}^{2-}$ remained intact (Figure 8).

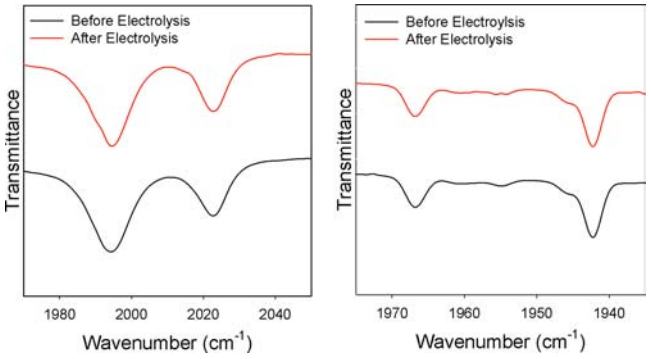

Figure 8. IR spectra of $\mathbf{1}^{-}$ (left) and $\mathbf{2}^{2-}$ (right) recorded before (black) and after (red) CPE.

We attribute the effectiveness of the butterfly shaped clusters, $\mathbf{1}^{-}$ and $\mathbf{2}^{2-}$, to their ability to form protonated adducts at pH 5. We have shown electrochemically that, following one-electron reduction, $\mathbf{1}^{-}$ is protonated in aqueous solution to afford H$\mathbf{1}^{-}$, and CV scans of $\mathbf{2}^{2-}$ under various pH conditions indicated its reduction is proton coupled and afforded H$\mathbf{2}^{2-}$ (Chart 2). In contrast, we saw no evidence for protonation or proton coupled electron transfer events in the CVs of $\mathbf{3}^{2-}$ and $\mathbf{4}^{2-}$. We did see some evidence that $\mathbf{3}^{2-}$ and $\mathbf{4}^{2-}$ rearrange to $\mathbf{2}^{2-}$ at pH 5 over the course of hours, so it is even possible that some of the hydrogen detected from CPE experiments on $\mathbf{3}^{2-}$ and $\mathbf{4}^{2-}$ is actually generated by $\mathbf{2}^{2-}$.

Mechanism of Hydrogen Evolution. The mechanistic details for the reactions where $\mathbf{1}^{-}$ and $\mathbf{2}^{2-}$ behave as catalysts for hydrogen evolution can be discussed based on the pH dependent CV measurements described above. Observation of the intermediate H$\mathbf{1}^{-}$ at pH 5 suggests that formation of H$\mathbf{1}^{-}$ by reduction followed by subsequent protonation are the initial steps in a catalytic cycle for formation of H_2 (Scheme 1).

Scheme 1

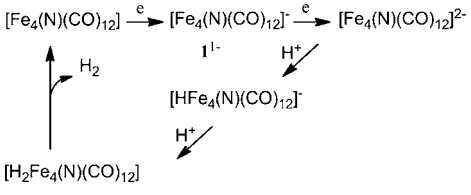

dx.doi.org/10.1021/ic4023882 | Inorg. Chem. 2013, 52, 12847−12854

Subsequent protonation of H$\mathbf{1}^-$ or bimolecular H_2 formation must be a slower step since we are able to experimentally observe build up of H$\mathbf{1}^-$. The pH dependence of this final step (as observed by the presence or absence of the redox wave for oxidation of H$\mathbf{1}^-$, vide supra) strongly implies that a second protonation event closes the catalytic cycle. This mechanism is also consistent with the first order dependence on concentration of $\mathbf{1}^-$ which we measured using CV (Supporting Information, Figure S6). We were unable to determine the order with respect to acid because the catalytic reaction is optimal only at pH 5. This proposed mechanism is consistent with the mechanism for hydrogen evolution MeCN solution that we have previously reported.[16]

The mechanism for catalysis of hydrogen evolution by $\mathbf{2}^{2-}$ is different from that described above for $\mathbf{1}^-$. Whereas $\mathbf{1}^-$ was protonated twice subsequent to its reduction to $\mathbf{1}^{2-}$, CV measurements indicated that $\mathbf{2}^{2-}$ undergoes two successive proton-coupled electron transfer events (Scheme 2): an initial

Scheme 2

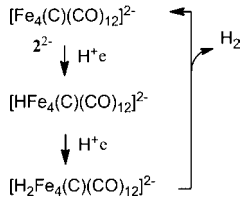

one proton, one electron step is followed by another one proton, one electron step and then liberatation of dihydrogen closes the catalytic cycle. This mechanism is also consistent with the first order dependence on concentration of $\mathbf{2}^{2-}$ which we measured using CV (Supporting Information, Figure S6).

Estimation of Catalytic Rates. The rate of the catalytic reactions performed by $\mathbf{1}^-$ and $\mathbf{2}^{2-}$ was estimated from the CV data collected over a range of scan rates, and analyzed using an approximation that describes the behavior of pseudo-first-order catalytic systems:

$$\frac{j_c}{j_p} = \frac{2}{0.466}\sqrt{\frac{RTk_{obs}}{F\nu}} \qquad (9)$$

where j_c is the catalytic current density, j_p is the noncatalytic current density, R is the ideal gas constant, T = 298.15 K, F = Faraday's constant, and υ = scan rate. This method for obtaining k_{obs} has been employed to analyze the rate constant of various hydrogen evolving electrocatalysts,[23] even though it rigorously represents a means to obtain rate constants only for simple pseudo-first-order systems with an *EC′* mechanism.[24] Approximations for k_{obs} can be obtained for system that have mechanisms more complicated than *EC′* and so we provide the information here to enable some comparison of these iron catalysts with other electrocatalysts that have been reported in the literature. For $\mathbf{2}^{2-}$ a value for k_{obs} was obtained using values for j_p that were taken from the reversible redox process observed for $\mathbf{2}^{2-}$ at −0.47 (pH 5), and values for j_c were obtained at −1.01 V vs SCE. The j_c values for $\mathbf{2}^{2-}$ are essentially scan-rate independent between 5 and 10 V/s, and the plot of j_c/j_p vs the inverse of the square root of the scan rate revealed a straight line between 5 and 10 V/s (Figure 9). From the slope of this line, k_{obs} was determined to be 368 s^{-1}.

No values of j_p could be obtained from the CVs of $\mathbf{1}^-$ because there are no noncatalytic redox events present. The

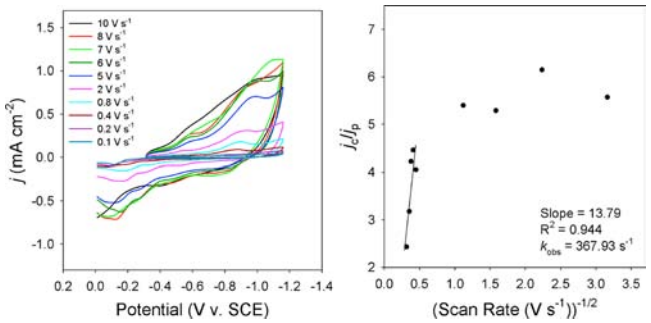

Figure 9. (left) CVs for [diglyme$_2$Na]$_2$-**2** recorded at scan rates between 0.1 and 10 v/s. GC electrode, pH 5. (right) Plot of j_c/j_p vs inverse of the square root scan rate taken from the left panel.

redox event at −1.25 V is a catalytic process and afforded us only values of j_c. The CVs recorded at scan rates from 0.1 up to 10 V/s for $\mathbf{1}^-$ did indicate that j_c is approximately scan rate independent above 3 V/s (Supporting Information, Figure S7). To obtain a very rough estimate of k_{obs} for $\mathbf{1}^-$ we compared the amount of charge passed in CPE experiments of both $\mathbf{1}^-$ and $\mathbf{2}^{2-}$. For $\mathbf{1}^-$ 68 C of charge were passed over 2 h whereas 38 C of charge were passed in the same time during catalysis by $\mathbf{2}^{2-}$. Multiplication of the k_{obs} value for $\mathbf{2}^{2-}$ by 68/38 affords an approximate value of k_{obs} for $\mathbf{1}^-$ which is 659 s^{-1}.

CONCLUSIONS

We have demonstrated that a series of low-valent iron clusters are active catalysts for hydrogen evolution at pH 5 at −1.25 V vs SCE. pH-dependent CV measurements indicated that the mechanism of hydrogen evolution by the butterfly shaped clusters containing nitride and carbide interstitial atoms consist of electrochemical and protonation events: the sequence of these events varies according to cluster charge. We propose that these protonated clusters are intermediates in the mechanism for hydrogen evolution and are essential for the observed efficient generation of hydrogen. In contrast, square pyramidal and octahedral carbide containing clusters do not associate with protons upon reduction, are inefficient for hydrogen evolution, and slowly rearrange to afford the butterfly shaped four iron cluster under acidic conditions.

The aqueous stability and relatively positive operating potential for hydrogen evolution by $\mathbf{1}^-$ and $\mathbf{2}^{2-}$ from aqueous solution are notable aspects of their function. These catalysts also compare very favorably with other first row transition metal electrocatalysts that effect hydrogen evolution from aqueous solution. These butterfly shaped clusters have very high Faradaic efficiencies, and they operate near neutral pH. Moreover, the range of operating potentials, from −1.1 to −1.25 V, and overpotential of 714 mV (pH 5), fall within the range of the most effective first row transition metal electrocatalysts, mainly cobalt- and nickel-based, reported to date. It is not possible to accurately compare the rates of catalysis based on the CPE measurements because factors such as CPE cell design, electrode surface area, and even electrode material vary greatly between reports available in the literature. However, the reports of charge passed during CPE measurements and our estimates of k_{obs} indicate that $\mathbf{1}^-$ and $\mathbf{2}^{2-}$ are efficient catalysts for hydrogen evolution in aqueous solution. Our future work will focus on further understanding the effects of cluster size, composition, and structure on H^+ and CO_2 reduction.

dx.doi.org/10.1021/ic4023882 | *Inorg. Chem.* 2013, 52, 12847−12854

EXPERIMENTAL SECTION

X-ray Structure Determination. X-ray diffraction studies were carried out on a Bruker SMART APEX Duo diffractometer equipped with a CCD detector.[25a] Measurements were carried out at −175 °C using Mo Kα (λ = 0.71073 Å) radiation. Crystals were mounted on a glass capillary or Kaptan Loop with Paratone-N oil. Initial lattice parameters were obtained from a least-squares analysis of more than 100 centered reflections; these parameters were later refined against all data. Data were integrated and corrected for Lorentz polarization effects using SAINT[25] and were corrected for absorption effects using SADABS2.3.

Space group assignments were based upon systematic absences, E statistics, and successful refinement of the structures. Structures were solved by direct methods with the aid of successive difference Fourier maps and were refined against all data using the SHELXTL 5.0 software package.[25] Thermal parameters for all non-hydrogen atoms were refined anisotropically. Hydrogen atoms, where added, were assigned to ideal positions and refined using a riding model with an isotropic thermal parameter 1.2 times that of the attached carbon atom (1.5 times for methyl hydrogens). One Level A Alert in the CIF file was observed: "PLAT029_ALERT_3_A _diffrn_measured_fraction_-theta_full Low.....0.939". This was due to an incorrect diffractometer setting. The installed 2θ maximum for the diffractometer was originally set below the actual maximum achievable value, and this is the primary reason the data have not been fully collected. This has little to no effect on the resulting structure.

Electrochemical Measurements. Cyclic voltammograms were recorded under a dinitrogen (99.998%, Praxair) atmosphere in Milli-Q water (18 MΩ) using either a CH Instruments Electrochemical Analyzer model 620D or a model 1100B, a glassy carbon working electrode (CH Instruments, nominal surface area of 0.0707 cm^2), a platinum wire auxiliary electrode, and a Ag/AgCl(sat.)/1 M KCl (Pine) reference electrode for aqueous experiments. Reported potentials are all referenced to the SCE couple, and were determined using ferrocene (Aldrich) as an internal standard where $E_{1/2}$ ferrocene/ferrocenium is +0.159 V vs SCE in water.[26] Phosphate buffer was used for pH 2, 7, and 11.4, acetate for pH 5, and borate for pH 9. Reagents for buffer preparation were purchased from EMD, VWR, and Sigma, and used as received. The supporting electrolyte was sodium perchlorate monohydrate ($NaClO_4 \cdot H_2O$) (Fisher Scientific) and was used as received. In all cases, CV sweeps were initiated at the open circuit potential and recorded in quiescent solution. No iR compensation was used for electrochemical measurements.

Controlled Potential Electrolyses. CPE experiments were performed in a gastight glass cell (working electrode compartment volume of 258 mL) under 1 atm of static dinitrogen (Praxair, 99.998%) with a stirred solution. The counter electrode compartment was separated from the working electrode compartment by a glass frit of medium porosity. In a typical experiment, 72 mL of degassed electrolyte solution were used in the working electrode compartment. Gas samples were injected directly in to a GC (see Other Physical Measurements). The working electrode was a glassy carbon plate with area 2.84 cm^2 (Tokai Carbon), while the counter electrode was a coiled Pt wire approximately 30 cm in length (BASi). The reference electrodes employed for CPE experiments were of similar design to those used for CV measurements. In between CPE experiments, the glass cell, the stir bar, the working electrode, and the counter electrode were cleaned by sonication in 3% (v/v) nitric acid for 5 min, rinsed with DI water, sonicated in DI water for 5 min, rinsed with DI water, and then sonicated in methanol for 5 min, rinsed with DI water, and then sonicated briefly in the solvent to be used during the next CPE experiment and allowed to dry in an oven before use. The glassy carbon plate had the additional, initial step of being thoroughly sanded on all surfaces with 300 grit SiC paper and then 600 grit SiC paper and rinsed with water prior to sonication steps.

Spectroelectrochemical measurements were performed using a gastight solution IR cell with CaF_2 windows, which could be loaded directly by attachment to the luer-lock syringe. Samples were taken before and after the CPE experiment using a gastight syringe, and loaded into the IR cell.

Other Physical Measurements. Elemental analyses were performed by Columbia Analytical. Infrared spectra were recorded on a Bruker Tensor Infrared spectrometer, and UV−vis spectra were collected in an air free manner using an HP 8452A Diode Array Spectrophotometer and a quartz cell (Starna) with a 1 cm path length. Quantitative measurement of H_2 was performed on a Varian 3800 GC equipped with a TCD detector and a Carboxen 1010 PLOT fused silica column (30 m × 0.53 mm) (Supelco) using dinitrogen (99.999%, Praxair) as the carrier gas. One-hundred microliter samples of the CPE atmosphere were extracted using a gastight syringe (Vici) and injected directly into the GC. H_2 concentration was determined using a previously prepared working curve. pH measurements of aqueous solutions were performed using a VWR SympHony pH meter with a posi-pHlo glass electrode. The estimated error for reported pH values is ±0.1 pH units. The meter was calibrated prior to use using a 3 point calibration with standard buffers (BDH) of pH 4, 7, and 10.

Preparation of Compounds. All manipulations were carried out using standard Schlenk or glovebox techniques under a dinitrogen atmosphere. Unless otherwise noted, solvents were deoxygenated and dried by thorough sparging with Ar gas followed by passage through an activated alumina column. Diglyme was purchased in a Sureseal bottle, degassed, and stored over activated 3 Å molecular sieves. Deuterated solvents were purchased from Cambridge Isotopes Laboratories, Inc. and were degassed and stored over activated 3 Å molecular sieves prior to use. $Na_2[Fe(CO)_4]$,[27] $[diglyme_2Na]_2[Fe_4(C)(CO)_{12}]$, $[Et_4N]_2[Fe_4(C)(CO)_{12}]$, $[DME_2Na]_2[Fe_5(C)(CO)_{15}]$, $[Et_4N]_2[Fe_5(C)(CO)_{15}]$, and $[DME_2Na]_2[Fe_6(C)(CO)_{18}]$ were prepared by methods similar to those reported in the literature. Synthesis of $[diglyme_2Na][Fe_4(N)(CO)_{12}]$ was adapted from a literature report and is described here because it is sufficiently different and because structural characterization was not previously reported.[11] All other reagents were purchased from commercial vendors and used without further purification.

$[(diglyme)_2Na][Fe_4(N)(CO)_{12}]$ ($diglyme_2$Na-1). Diglyme (70 mL) was added to a mixture of $Na_2[Fe(CO)_4]$ (6.6 g, 31.43 mmol) and $Fe(CO)_5$ (32.0 g, 163 mmol). The reaction was stirred for 2 h and then $NOBF_4$ (3.60 g, 30.8 mmol) was slowly added. The solution was heated to 160 °C or reflux for 2 h and then cooled. Hexane (ca. 100 mL) was added to afford a black precipitate which was isolated by removal of the supernatant via cannula. The black precipitate was washed with water (3 × 100 mL), and then extracted into dry DCM (50 mL). Ethanol (50 mL) was added into the DCM solution, and the volume of the solvent reduced by half under vacuum. The solution was stored at −20 °C for one week to afford 12.0 g of **1** as a black crystalline powder (75% yield). Crystals suitable for single crystal X-ray diffraction could be grown by evaporation of a H_2O-THF (v/v 9:1) solution of **1**. IR spectrum: υ_{CO} 2016(s), 1987(s), 1965(m), 1930(m) cm^{-1}. Anal. Calcd. for $C_{24}H_{28}O_{18}NNaFe_4$: C, 33.33; H, 3.26; N, 1.62. Found: C, 33.62; H, 3.45; N, 1.46. UV−vis spectrum (H_2O): λ_{max} (ε_M): 294 nm (43,000), (sh) 352 nm (18,000), (sh) 580 (900) nm (L mol^{-1} cm^{-1}).

ASSOCIATED CONTENT

Supporting Information

Crystallographic tables, CPE results, NMR spectra, and plots of CV measurements. This material is available free of charge via the Internet at http://pubs.acs.org.

AUTHOR INFORMATION

Corresponding Author

*E-mail: laberben@ucdavis.edu.

Author Contributions

†These authors contributed equally. All authors have given approval to the final version of the manuscript.

Notes

The authors declare no competing financial interest.

■ ACKNOWLEDGMENTS

This work was supported by UC Davis and NSF CAREER (CHE-1055417 and CHE-1340203). L.A.B. is an Alfred P. Sloan Foundation Fellow. A.D.N. thanks UC LEADS and a Provost Undergraduate Fellowship for partial support. We thank T.W. Myers for experimental assistance with the synthesis of clusters.

■ REFERENCES

(1) For example: (a) Houlding, V.; Geiger, T.; Kölle, U.; Grätzel, M. *J. Chem. Soc., Chem. Commun.* **1982**, 681. (b) Collin, J. P.; Jouaiti, A.; Sauvage, J. P. *Inorg. Chem.* **1988**, *27*, 1986. (c) Bernhardt, P. V.; Jones, L. A. *Inorg. Chem.* **1999**, *38*, 5086. (d) Abdel-Hamid, R.; El-Sagher, H. M.; Abdel-Mawgoud, A. M.; Nafady, A. *Polyhedron* **1998**, *17*, 4535. (e) Stubbert, B. D.; Peters, J. C.; Gray, H. B. *J. Am. Chem. Soc.* **2011**, *133*, 18070. (f) Sun, Y.; Bigi, J. P.; Piro, N. A.; Tang, M. L.; Long, J. R.; Chang, C. J. *J. Am. Chem. Soc.* **2011**, *133*, 9212. (g) Karunadasa, H. I.; Montalvo, E.; Sun, Y.; Majda, M.; Long, J. R.; Chang, C. J. *Science* **2012**, *335*, 698. (h) McCrory, C. C. L.; Uyeda, C.; Peters, J. C. *J. Am. Chem. Soc.* **2012**, *134*, 3164. (i) Singh, W. M.; Baine, T.; Kudo, S.; Tian, S.; Ma, X. A. N.; Zhou, H.; DeYonker, N. J.; Pham, T. C.; Bollinger, J. C.; Baker, D. L.; Yan, B.; Webster, C. E.; Zhao, X. *Angew. Chem., Int. Ed.* **2012**, *24*, 5941. (j) Thoi, V. S.; Sun, Y.; Long, J. R.; Chang, C. J. *Chem. Soc. Rev.* **2013**, *42*, 2388. (k) Pool, D. H.; Stewart, M. P.; Stewart, M. P.; O'Hagan, M. P.; Shaw, W. J.; Roberts, J. A. S.; Bullock, R. M.; DuBois, D. L. *Proc. Natl. Acad. Sci. U.S.A.* **2012**, *109*, 15634. (l) McNamara, W. R.; Han, Z.; Yin, C.-J. M.; Brennessel, W. W.; Holland, P. L.; Eisenberg, R. *Proc. Natl. Acad. Sci. U.S.A.* **2012**, *109*, 15594.

(2) Bhugun, I.; Lexa, D.; Savéant, J.-M. *J. Am. Chem. Soc.* **1996**, *118*, 3982.

(3) (a) Kaur-Ghumaan, S.; Schwartz, L.; Lomoth, R.; Stein, M.; Ott, S. *Angew. Chem., Int. Ed.* **2010**, *49*, 8033. (b) Schwartz, L.; Singh, P. S.; Eriksson, L.; Lomoth, R.; Ott, S. *C. R. Chim.* **2008**, *11*, 875.

(4) Rose, M. J.; Gray, H, B. *J. Am. Chem. Soc.* **2012**, *134*, 8310.

(5) Felton, G. A. N.; Mebi, C. A.; Petro, B. J.; Vannucci, A. K.; Evans, D. H.; Glass, R. S.; Lichtenberger, D. L. *J. Organomet. Chem.* **2009**, *694*, 2681.

(6) For example: (a) Hsieh, C. H.; Erdem, O. F.; Harman, S. D.; Singleton, M. L.; Reijerse, E.; Lubitz, W.; Popescu, C. V.; Reibenspies, J. H.; Brothers, S. M.; Hall, M. B.; Darensbourg, M. Y. *J. Am. Chem. Soc.* **2012**, *134*, 13089. (b) Felton, G. A. N.; Vannucci, A. K.; Chen, J.; Lockett, L. T.; Okumura, N.; Petro, B. J.; Zakai, U. I.; Evans, D. H.; Glass, R. S.; Lichtenberger, D. L. *J. Am. Chem. Soc.* **2007**, *129*, 12521. (c) Wang, W.; Rauchfuss, T. B.; Bertini, L.; Zampella, G. *J. Am. Chem. Soc.* **2012**, *134*, 4525. (d) Liu, T.; Wang, M.; Shi, Z.; Cui, H.; Dong, W.; Chen, J.; Akermark, B.; Sun, L. *Chem.—Eur. J.* **2004**, *10*, 4474.

(7) For example: Mejia-Rodriguez, R.; Chong, D.; Reibenspies, J. H.; Soriaga, M. P.; Darensbourg, M. Y. *J. Am. Chem. Soc.* **2004**, *126*, 12004.

(8) Le Cloirec, A.; Davies, S. C.; Evans, D. J.; Hughes, D. L.; Pickett, C. J.; Best, S. P.; Borg, S. *Chem. Commun.* **1999**, 2285.

(9) (a) Singleton, M. L.; Reibenspies, J. H.; Darensbourg, M. Y. *J. Am. Chem. Soc.* **2010**, *132*, 8870. (b) Singleton, M. L.; Crouthers, D. J.; Duttweiler, R. P.; Reibenspies, J. H.; Darensbourg, M. Y. *Inorg. Chem.* **2011**, *50*, 5015.

(10) (a) Quentel, F.; Passard, G.; Gloaguen, F. *Chem.—Eur. J.* **2012**, *18*, 13473. (b) Quentel, F.; Passard, G.; Gloaguen, F. *Energy Env. Sci.* **2012**, *5*, 7757.

(11) (a) Tachikawa, M.; Stein, J.; Muetterties, E. L. *J. Am. Chem. Soc.* **1980**, *102*, 6648. (b) Fjare, D. E.; Gladfelter, W. L. *J. Am. Chem. Soc.* **1981**, *103*, 1572.

(12) Strong, H.; Krusic, P. J.; Filippo, J. S.; Keenan, S.; Finke, R. G. Sodium Carbonyl Ferrates, $Na_2[Fe(CO)_4]$, $Na_2[Fe_2(CO)_8]$, and $Na_2[Fe_3(CO)_{11}]$. Bis[μ-Nitrido-Bis(Triphenylphosphorus)(1^+)] Undeca-Carbonyltriferrate(2^-), $[(Ph_3P)_2N]_2[Fe_3(CO)_{11}]$. In *Inorganic Syntheses: Reagents for Transition Metal Complex and Organometallic Syntheses*; Angelici, R. J., Ed.; John Wiley & Sons, Inc.: Hoboken, NJ, 2007; Vol. *28*.

(13) Tachikawa, M.; Geerts, R. L.; Muetterties, E. L. *J. Organomet. Chem.* **1981**, *213*, 11.

(14) Kolis, J. W.; Drezdzon, M. A.; Shriver, D. F. *Inorg. Synth.* **1989**, *26*, 246.

(15) Bard, A. J.; Faulkner, L. R. *Electrochemical Methods: Fundamentals and Applications*, 2nd ed.; Wiley: New York, 2001.

(16) Rail, M. D.; Berben, L. A. *J. Am. Chem. Soc.* **2011**, *133*, 18577.

(17) Corresponding redox events at pH 7 and 9 were not observed which is likely due to the higher capacitive current we observed at these pH values.

(18) pH dependence of the redox events can be understood by reference to the Nernst equation. Bard, A. J.; Faulkner, L. R. *Electrochemical Methods: Fundamentals and Applications*, 2nd ed.; Wiley: New York, 2001; p 31.

(19) Beno, M. A.; Williams, J. M.; Tachikawa, M.; Muetterties, E. L. *J. Am. Chem. Soc.* **1980**, *102*, 4542.

(20) (a) Zaffaroni, R.; Rauchfuss, T. B.; Fuller, A.; De Gioia, L.; Zampella, G. *Organometallics* **2013**, *32*, 232. (b) Wang, W.; Nilges, M. J.; Rauchfuss, T. B.; Stein, M. *J. Am. Chem. Soc.* **2013**, *135*, 3633. (c) Manor, B. C.; Rauchfuss, T. B. *J. Am. Chem. Soc.* **2013**, *135*, 11895.

(21) Tachikawa, M.; Muetterties, E. L. *J. Am. Chem. Soc.* **1980**, *102*, 4541.

(22) Overpotential is the difference between the operating potential of the CPE experiment and the thermodynamic potential for H_2 evolution at the pH specified in the text. For $2H^+ + 2e \rightarrow H_2$, thermodynamic potential is given by $E(\mathrm{pH}) = -0.241\ \mathrm{V} - 0.059\ \mathrm{V}(\mathrm{pH})$.

(23) For example: (a) Hu, X.; Brunschwig, B. S.; Peters, J. C. *J. Am. Chem. Soc.* **2007**, *129*, 8988. (b) Bigi, J. P.; Hanna, T. E.; Harman, W. H.; Chang, A.; Chang, C. J. *Chem. Commun.* **2010**, *46*, 958. (c) Kilgore, U. J.; Roberts, J. A. S.; Pool, D. H.; Appel, A. M.; Stewart, M. P.; DuBois, M. R.; Dougherty, W. G.; Kassel, W. S.; Bullock, R. M.; DuBois, D. L. *J. Am. Chem. Soc.* **2011**, *133*, 5861. (d) Appel, A. M.; Pool, D. H.; O'Hagan, M.; Shaw, W. J.; Yang, J. Y.; Rakowski DuBois, M.; DuBois, D. L.; Bullock, R. M. *ACS Catal.* **2011**, *1*, 777. (e) Stubbert, B. D.; Peters, J. C.; Gray, H. B. *J. Am. Chem. Soc.* **2011**, *133*, 18070.

(24) (a) Saveant, J. M.; Vianello, , E. *Electrochim. Acta* **1965**, *10*, 905. (b) Saveant, J. M.; Vianello, E. *Electrochim. Acta* **1967**, *12*, 629. (c) Andrieux, C. P.; Dumas-Bouchiat, J. M.; Saveant, J. M. *J. Electroanal. Chem.* **1980**, *113*, 2348. (d) Saveant, J.-M. *Chem. Rev.* **2008**, *108*, 2348.

(25) (a) *SMART Software Users Guide*, Version 5.1; Bruker Analytical X-Ray Systems, Inc.: Madison, WI, 1999. (b) *SAINT Software Users Guide*, Version 7.0; Bruker Analytical X-Ray Systems, Inc.: Madison, WI, 1999. (c) Sheldrick, G. M. *SADABS*, Version 2.03; Bruker Analytical X-Ray Systems, Inc.: Madison, WI, 2000. (d) Sheldrick, G. M. *SHELXTL*, Version 6.12; Bruker Analytical X-Ray Systems, Inc.: Madison, WI, 1999. (e) *International Tables for X-Ray Crystallography*; Kluwer Academic Publishers: Dordrecht, The Netherlands, 1992; Vol. *C*.

(26) (a) Noviandri, I.; Brown, K. N.; Fleming, D. S.; Gulyas, P. T.; Lay, P. A.; Masters, A. F.; Phillips, L. *J. Phys. Chem. B* **1999**, *103*, 6713. (b) Bard, A. J.; Faulkner, L. R. *Electrochemical Methods: Fundamentals and Applications*, 2nd ed.; Wiley: New York, 2001.

(27) Strong, H.; Krusic, P. J.; Filippo, J. S.; Keenan, S.; Finke, R. G. Sodium Carbonyl Ferrates, $Na_2[Fe(CO)_4]$, $Na_2[Fe_2(CO)_8]$, and $Na_2[Fe_3(CO)_{11}]$. Bis[μ-Nitrido-Bis(Triphenylphosphorus)(1^+)] Undeca-Carbonyltriferrate(2^-), $[(Ph_3P)_2N]_2[Fe_3(CO)_{11}]$. In *Inorganic Syntheses: Reagents for Transition Metal Complex and Organometallic Syntheses*; Angelici, R. J., Ed.; John Wiley & Sons, Inc.: Hoboken, NJ, 2007; Vol. *28*.